Light-Sheet Skew-Ray Enhanced Pump-Absorption for Sensing

George Y. Chen ⓘ, Alexandre François ⓘ, Xuan Wu, Wen Qi Zhang ⓘ, Christophe A. Codemard, Haolan Xu ⓘ, Tanya M. Monro ⓘ, and David G. Lancaster ⓘ

Abstract—We present a new sensing technique exploiting light-sheet excitation of skew rays in a multimode fiber, which can be applied to enhance the sensitivity of a range of sensing mechanisms such as pump absorption. The underlying principle is that a light sheet (i.e., thin plane of light) can selectively concentrate the optimum ray group, giving rise to enhanced interaction between light and matter (e.g., fluorophores). We compared this excitation method with others in terms of attenuation of pump light through Rhodamine B. It was observed that the attenuation experienced by light-sheet skew rays can be up to one order of magnitude higher than that of collimated skew rays, and three orders of magnitude higher than that of normal-incidence rays.

Index Terms—Enhancement, light sheet, multimode fiber, pump absorption, sensing, skew rays.

I. INTRODUCTION

PUMP absorption and fluorescence [1]–[8] are well established sensing mechanisms for the detection and quantification of biological or chemical measurands for the applications of healthcare, manufacturing and security. Multimode fibers have been widely adopted for delivering light and probing local environments in evanescent-wave-based bio/chemical sensors, due to their high simplicity, high robustness and commercial availability at a low cost. A stronger pump absorption is desirable, because it increases the sensitivity, and thus improves the detection limit/accuracy. In response, excitation of high-order modes in multimode fibers with focused rays or collimated skew rays to strengthen light-matter interaction have been investigated, but only led to limited enhancements in pump absorption due to unoptimized ray groups [9]–[12]. Enhancements up to ~19 dB
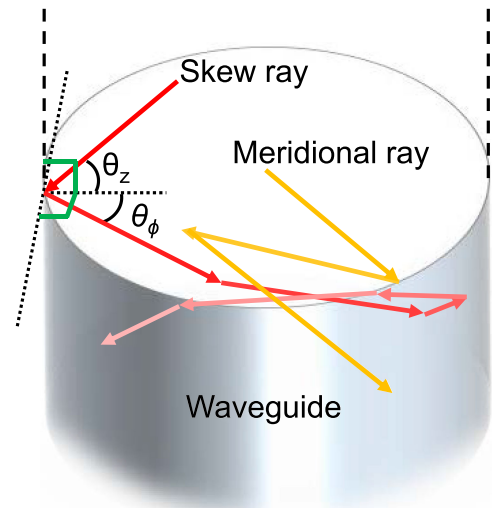
Fig. 1. Illustration of the different ray types in a cylindrical multimode waveguide such as an optical fiber.

relative to normal-incidence rays have been reported from using rays resulting from using a tilted fiber with focused and centered rays in a 320 μm core diameter [9]. To increase the evanescent interaction between light and matter (e.g., fluorophores) for bio/chemical sensing, we present a new sensing technique based on light-sheet skew rays (LSSR), and compare it with existing excitation methods in terms of attenuation of pump light through Rhodamine B. This is an advancement on the sensing platform comprising low refractive-index coated all-core/rod-type multimode fibers interrogated by skew rays [13]–[17]. The aim with LSSR is to tailor the ray groups such that only the rays with the most sensitive incident angle are used and evenly distributed along the core-external interface of the sensing fiber for interacting with fluorophores. This is an inline configuration based on commercial optics and multimode fibers that can be highly sensitive, relatively temperature insensitive, and highly robust.

II. PRINCIPLES

Skew rays do not cross the axis of the waveguide, and are excited when rays reflect off a curved boundary. They exhibit two angles relative to the core-cladding interface seen from the longitudinal and transverse perspectives, as shown in Figure 1. They are similar to orbital-angular-momentum modes [18],

except they can be fine-tuned at a lower cost. Skew rays enable a larger number of total internal reflections (N_r) than meridional rays for the same launch angle (θ), as shown in Equation 1 [19], which can enhance the sensitivity of numerous sensing mechanisms such as optical-confinement absorption, molecular (e.g., pump) absorption and fluorescence.

$$N_r = 1/\left(\left[\frac{2R\cos\theta_\phi}{\cos\theta_z} + d\right] \cdot \sin\theta_z\right) \quad (1)$$

where R is the fiber core radius (i.e., cladding is the functional coating); d is the penetration length per reflection (i.e., Goos–Hänchen shift); $\theta_z = \frac{\pi}{2} - \sin^{-1}(\frac{\sin\theta}{n})$ is the angle between the ray and the normal of the core-cladding interface seen from the transverse perspective; $\theta_\phi = \frac{\pi}{2} - \cos^{-1}(\frac{i}{N})$ is the angle between the ray and the normal of the core-cladding interface seen from the longitudinal perspective, which represents skewness; n is the refractive index of the optical fiber; i represents the fractional step offset from the center of the fiber; and N represents the total number of steps from the center to the edge of the optical fiber.

Skew rays can also be excited at θ much greater than the upper limit of meridional rays. Furthermore, sensing mechanisms based on the total power of light (i.e., not always affected by the thermo-optic effect), such as in this case, are far more temperature insensitive compared to interferometric techniques (i.e., strongly affected by the thermo-optic and thermal expansion effects) based on the phase of light.

To elaborate, skew rays host larger numbers of reflections compared to that of meridional rays under the same θ, which can be a few orders of magnitude higher, as well as longer penetration lengths. This facilitates a longer total penetration path length inside a functional coating or an external medium (i.e., higher sensitivity to uniform external changes [20]–[22]), and a better circular coverage around the circumferential surface of the sensing fiber (i.e., higher probability of encountering point perturbations [23], and higher measurement-repeatability or better measurand averaging with non-uniform analytes) unless meridional rays are focused and centered. However, meridional rays pack larger portions of power in their evanescent fields due to smaller incident angles, which boosts the sensitivity. For all rays, higher order (i.e., smaller θ_z or larger θ) leads to longer optical path lengths and thus more significant mode dispersion and mode diffusion, which deteriorates the ray-group purity. Hence, medium-order (i.e., medium θ_z or θ) skew rays of low skewness (i.e., θ_ϕ or small center offset) possess the key benefits of all types, being able to achieve and maintain similar penetration depths to meridional rays while hosting far more reflections inherent to skew rays, and thus exhibit higher sensitivity.

To determine a relationship between the measurand (i.e., dye concentration) and the detected parameter (i.e., attenuation, positive form) and thus provide future readouts of the dye concentration, θ and core offset are swept for each concentration step while the residual pump power is collected for calculating the corresponding attenuation. The residual pump power is chosen instead of the fluorescence intensity due to the higher output coupling efficiency. Better fluorescence collection is possible with a higher fiber numerical-aperture (>0.5) or a fiber

bundle. The calibration graph for the end-user is obtained from the relationship between dye concentration and attenuation based on the optimum launch conditions. The sensitivity (i.e., attenuation/dye concentration) is equal to the gradient of the calibration graph, and the detection limit/accuracy (i.e., dye concentration) is calculated from dividing the noise-equivalent attenuation by the sensitivity.

Dye concentration is used instead of a measurand for the purpose of demonstration, which is linearly proportional to attenuation [24], and typically inversely proportional to the measurand [3]. The detection limit of the dye concentration corresponds to the detection limit/accuracy of the measurand.

For attenuation, the residual pump power is normalized by the baseline optical power (i.e., received optical power when Milli-Q pure water is used instead of the dye), due to several reasons: (a) The more direct relationship improves reproducibility and facilitates fairer comparisons to other systems; (b) The change in the input optical power due to the Lambertian Cosine Law and shifting segment of illumination can be compensated by adjusting the source optical power (i.e., typically low cost) or mathematical scaling via division with a baseline measurement which is linearly proportional to the input optical power; and (c) Below saturation, residual pump power is linearly proportional to the input optical power used for excitation, and thus can be scaled together. Unlike the input coupling efficiency between source and input optical powers, the output coupling efficiency between output optical power and received optical power affects sensitivity. However, an integrating sphere or a large-core high numerical-aperture multimode fiber leading to a spectrometer can collect most of the residual pump light to maximize the signal-to-noise ratio.

The proposed sensing technique exploits the high selectivity of light sheets within collimated skew rays. Generally, for sensitivity optimization, there are 7 stages after choosing the measurand and sensing mechanism: wavelength, fiber diameter, coating thickness/concentration, θ_ϕ, θ_z, fiber length, and polarization azimuth. Re-optimization is required for changes in fiber dimensions/geometry/materials/bend angles.

The fluorophores of Rhodamine B dissolved in water absorbs a certain wavelength band and reemits at a longer wavelength band as fluorescence. A wavelength of 532 nm was selected for efficient pump absorption.

Enlarging the fiber diameter has counteracting effects, but ultimately proves beneficial. When the detected parameter is based on pump power, the detection limit/accuracy is inversely proportional to the signal-to-noise ratio. Since the dominant noise source tends to be shot noise (i.e., proportional to square root of the optical power) for non-interferometric sensing mechanisms, increasing the fiber diameter increases the input optical power by area, and increases the noise-equivalent power linearly. Therefore, the signal-to-noise ratio increases linearly with increasing fiber diameter. On the other hand, Equation 1 shows that increasing the fiber diameter decreases the number of reflections, the total penetration path length and thus the sensitivity, which offsets the first detection-limit enhancement. Moreover, a larger fiber diameter allows a finer selection of ray groups when the input fiber end-face is not completely spatially filled with light,
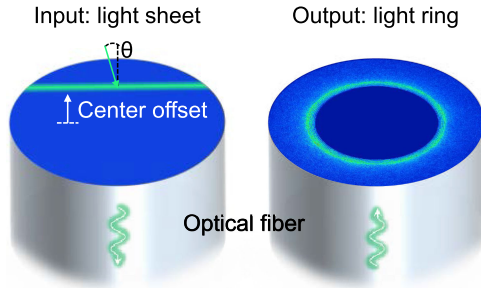
Fig. 2. Illustration of light sheet excitation of an optical fiber, which results in a narrow light ring at the output end, due to the fiber curvature and tilt introducing a continuum of delays to different segments of the input light sheet.

which can optimize the sensitivity (i.e., see light sheets below). The upper limit to the ideal fiber diameter depends on the application, with fiber flexibility and compactness taken into account. A fiber diameter of 320 μm was used to provide a good balance between such attributes.

It is worth noting that thin-walled capillaries excited with non-meridional rays can also offer several orders of magnitude improvement in sensitivity [25], due to the strong evanescent field overlapping with the surroundings. However, hollow structures are more mechanically unstable. Thick-walled capillaries excited with focused and centered rays offer slightly better stability, and can support highly sensitive meridional rays due to the wall geometry increasing the number of reflections.

For the purpose of demonstration, a dye bath was used to embed the sensing fiber instead of a dye-doped coating. A relatively high Rhodamine B concentration of 1 mg/ml was chosen to produce significant reabsorption of residual pump light. As a result, a longpass filter to remove fluorescence is not required, which avoids the complexity of calculating the variable insertion loss. Even this level of dye concentration produces a negligible increase in the refractive index [26] of pure water, and thus a negligible optical confinement loss in the tested range of θ that would otherwise make attenuation measurements unreliable.

Using a collimated light sheet instead of a collimated beam enables a higher sensitivity, especially for thinner light sheets illustrated in Figure 2. This is because there is an optimum skewness of rays that maximizes their interaction with the functional coating exposed to the measurand, considering the total penetration path length, and the portion of power in their evanescent fields. While it is an average effect with a collimated beam due to the mixture of rays, it is a precise selection with a light sheet to pick out and amplify the dominant contributor to the sensitivity. In addition, the narrower the ray group, the weaker the pump absorption instability associated transverse mode competition [27].

Fine tuning of θ_ϕ (i.e., via center-offset of light sheet) followed by θ_z (i.e., via θ) will optimize the ray skewness to maximize the evanescent-field interaction with the water molecules in the PEM and thus the sensitivity. Varying the center angle of θ_ϕ involves vertical translation of the horizontal light-sheet incident on the input fiber end-face. It is ideal to have the narrowest possible angle range by reducing the light-sheet thickness. However, it is difficult to achieve a collimated light sheet with

a thickness below a few hundred microns, due to fundamental diffraction limit associated with collimating to a small beam diameter [28]. It is also not possible to facilitate the propagation of a segmented Bessel beam [29], due to the curved geometry and the initial air-to-glass aperture breaking the phase conditions. To approximate a collimated light sheet with minimized sheet thickness and divergence angle, a cylindrical plano-convex lens can be used after a collimator plano-convex lens. Less-divergent thicker sheets start thicker (i.e., at the fiber input) and the larger sampled fiber curvature grows their thickness even further. More-divergent thinner sheets start thinner but grow more rapidly in sheet thickness. Focal lengths of 200 mm and 300 mm were employed for the cylindrical and non-cylindrical lenses to deliver a good balance between such characteristics, which produced thinner output light-rings than other lens combinations. The focal point should be positioned just inside (e.g., 5 mm) the input fiber end-face to minimize the light-sheet thickness, otherwise converging/diverging rays entering the sensing fiber take very different circular paths and broaden the light ring seen at the fiber output. It was found that within a focal-spot position tolerance of ± 5 mm there is negligible difference in the output light-ring thickness, due to the interplay between the input light-sheet thickness, angle and diffraction. Aligning the middles of the sensing fiber and the beam (i.e., approximately rectangular overlap with fiber) offers better mechanical stability and rotation-center tolerance. For each θ_ϕ, the range of θ_z can be swept for data collection. The effective incident angle is a function of both angles:

$$\gamma = \cos^{-1}\left[\cos\theta_z \cos\theta_\phi\right] \qquad (2)$$

Mode dispersion (i.e., geometrical gradients, chromatic dispersion) and mode diffusion (i.e., Rayleigh scattering, birefringence) increase with increasing optical path length of light along the sensing fiber, which convert LSSR from a thin-line input to a thick-ring output. While this increases circular coverage, it lowers the ray-group purity. The fiber length before the sensing window was chosen to be 35 cm for good balance between circular coverage and ray-group purity within the tested range of θ. The fiber length after the sensing window was selected to be 31 cm for preventing small bend radii. Fiber length was not included in the previous θ_ϕ and θ_z permutations to minimize the complexity of optimization.

Lastly, the polarization azimuth of linearly polarized light can be tailored to deliver high sensitivity via a good balance between penetration depth and transmission. The polarization azimuth was not included in the previous θ_ϕ and θ_z permutations to avoid increasing the complexity of optimization.

III. EXPERIMENTAL SETUP

Figure 3 shows the schematic of the experimental setup used to launch pump light via different excitation methods through the sensing fiber partially immersed in Rhodamine B. To probe the sensing fiber (SPI Lasers, coated silica rod fiber, Ø320 μm, 0.4 NA, 70 cm length, ~40 cm bend radius), an unpolarized single-mode 532 nm laser source (Thorlabs DJ532-40, LTC56B, LDC205C, TED200C) was used. The source
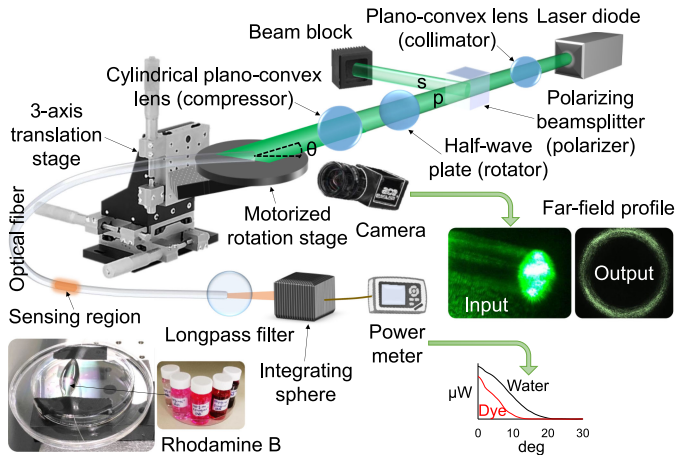
Fig. 3. Experimental setup for producing light-sheet skew rays. Note: longpass filter is only used for wavelength verification, not measurements.
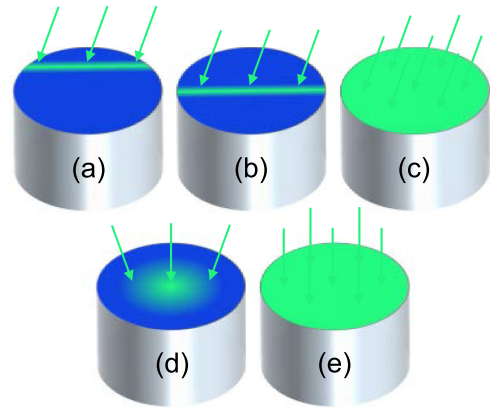

Fig. 4. Illustration of: (a) Light-sheet skew rays. (b) Collimated meridional rays. (c) Collimated skew rays. (d) Focused rays. (e) Normal-incidence rays.

optical power was regulated using a variable attenuator based on a wheel of neutral-density discs. Collimation of pump light (3.6 mm beam diameter) was achieved using a plano-convex lens of 300 mm focal length. The state and azimuth of polarization were controlled with a polarizing beamsplitting cube (i.e., transmits P-polarization relative to the plane of fiber rotation) and a half-wave plate (i.e., 45° for all comparisons, S-polarization) respectively. To produce a light sheet (∼40 μm input light-sheet thickness, 8.4 mm Rayleigh range, output light-ring thickness is difficult to measure via near-field projection due to skew ray angles), a removable cylindrical plano-convex lens of 200 mm focal length was employed. The flat-cleaved input end of the sensing fiber was mounted on a motorized rotation stage (Thorlabs CR1/M-Z7) at the center of rotation.

The input optical power and thus the signal-to-noise ratio limit were maximized (i.e., improves detection limit/accuracy) by centering the collimated beam on the input end of the sensing fiber, via a 3-axis translation stage which holds the rotation stage. Note, θ is varied horizontally while the center offset is varied vertically, as shown in Figure 2. The light entering the sensing fiber from the sides do not propagate far due to refraction allowing them to escape the fiber. Light entered through the input fiber end-face was guided only in the core, because the cladding is highly lossy from exposure to high-RI materials on the fiber mount. There was negligible light entered through the side of the fiber due to reflective and refractive effects. To visually monitor the position of a light sheet on the input end-face of the sensing fiber, a camera/lens was employed (Basler Ace acA1920-25uc, Computar MLH-10X). The sensing fiber projected the output light into an integrating-sphere power meter (Thorlabs S142C, PM100D, each data point from 100 samples or 300 ms integration time). A 570 nm longpass colored-glass filter (Thorlabs FGL570) was used to verify the negligible fluorescence received by the power meter for all θ, and thus the total received optical power is all residual pump power. Therefore, the filter was not used for the measurements. The absence of received fluorescence is due to fluorescence reabsorption, as well as the slightly higher water-absorption loss for fluorescence (580 nm) than pump light (532 nm). All attenuation measurements are repeated for dye (i.e., excitation comparison) and pure water (i.e., baseline).

IV. SENSING FIBER PREPARATION

The sensing fiber was window stripped (i.e., abrupt strip edges) by removing a coating section of 40 mm length with a surgical blade. Such a length was chosen to sample an average concentration if the distribution of dye is non-uniform. The bare-fiber region was then cleaned using isopropanol and lint-free wipes. The resulting sensing fiber features a 35 cm long pristine-section, 4 cm long bare/sensing section, and 30 cm long pristine-section. To provide a low-friction mobile bath of Rhodamine B such that it does not restrict the movement of the sensing fiber under rotation, the resulting section of bare fiber is suspended by two metal discs and fixed on top of a plastic petri dish cover using adhesive tape. The cover was floated on water inside a larger petri dish, as shown in in Figure 3. A sufficient volume of diluted Rhodamine B (1 mg/ml dissolved in Milli-Q pure water) was deposited on the bare-fiber region to fully immerse it. The dye was confined within the proximity of the fiber due to the hydrophobic petri dish surface. For baseline optical power measurements, pure water is used instead of the dye employed for excitation measurements.

V. RESULTS AND DISCUSSIONS

To facilitate a comparison, several common excitation types including the new LSSR were tested as shown in Figure 4, which includes LSSR, collimated meridional rays, collimated skew rays, focused-centered rays and normal-incidence rays.

The setup shown in Figure 3 was used to conduct both LSSR and collimated meridional-ray measurements (i.e., equivalent to LSSR with zero centre-offset). The attenuation (10 × absorbance) between the dye and pure-water measurements are plotted in Figure 5, as a function of θ and the center offset of the light sheet. For LSSR, their two highest peaks of attenuation are 34.9 dB and 32.0 dB, which can be seen at ($\theta = 20.0$ deg, 12.5 μm center offset) and ($\theta = 17.0$ deg, 112.5 μm center offset) respectively. The results inform of maximum attenuation with a mid-range θ and a slight center offset. The launch angle
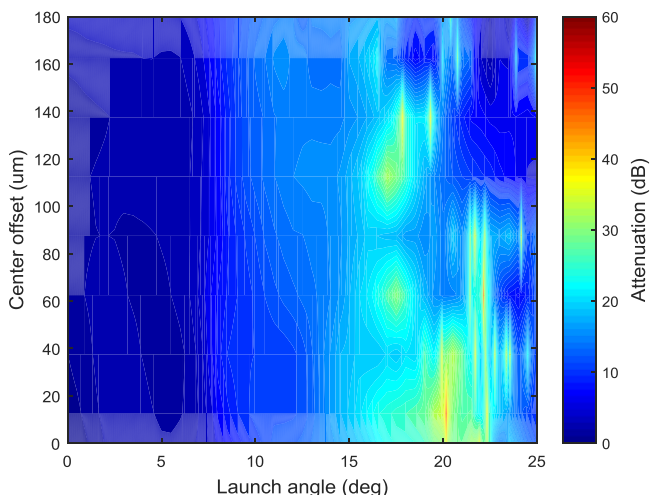
Fig. 5.   Measured attenuation of light-sheet skew rays as a function of launch angle and center offset. Angle step size is 0.5 deg, offset step size is 25 μm. Note: color values are not accurate due to MATLAB's curve fitting.

Fig. 6.   Measured attenuation of collimated skew rays as a function of launch angle.

errors are negligible, while the center offset errors are ± 5 μm. It is possible that higher enhancements occur at larger θ or center offset, but the range of input optical powers used that avoids photobleaching for Rhodamine B goes down into the noise floor.

It is apparently from the lack of symmetries or continuous peaks in Figure 5 that the center offset (i.e., affects θ_ϕ) and θ (i.e., affects θ_z) are not interchangeable despite their common contribution to γ inside the sensing fiber. This is because the relationship between center offset and θ_ϕ is nonlinear, unlike the linear relationship between θ and θ_z. As a result, a mid-range θ is matched to a large center-offset close to the top/bottom fiber edge. Hence, the relatively large curvature experienced by the light sheet creates a mixture of ray groups with various detuning from the desired effective angle. From Figure 5, the angle-dependent attenuation of collimated meridional rays can be found at zero center-offset. Their highest peak of attenuation is lower at 30.2 dB ($\theta = 21.5$ deg). It can be seen that a significant reduction in attenuation occurs beyond the critical angle of $\theta = 23.5$ deg, where a considerable portion of the propagating optical power is lost through meridional rays.

The setup shown in Figure 3 was modified for producing both collimated skew rays and normal-incidence rays (i.e., equivalent to collimated skew rays with 0 deg), by removing the cylindrical lens. By varying θ alone, the results are shown in Figure 6. For collimated skew rays, their highest two peaks of attenuation are 21.2 dB and 17.2 dB, which can be found at 20.0 deg and 15.5 deg respectively. Similarly, it shows that the maximum attenuation is associated with a mid-range θ. As anticipated, the optimum θ occurs at 20.0 deg, which shows excellent agreement with the LSSR that serves to fine tune the optimum ray group. From Figure 6, the attenuation of normal-incidence rays can be seen at $\theta = 0$ deg, which is lower at 0.9 dB. The repeatability ranges from 9% to 77%, which correspond to attenuation error bars between ± 0.8 dB and ± 8.9 dB. The worse repeatability at higher θ arise from lower levels of transmitted power, which are comparable to and sometimes dominated by noise.
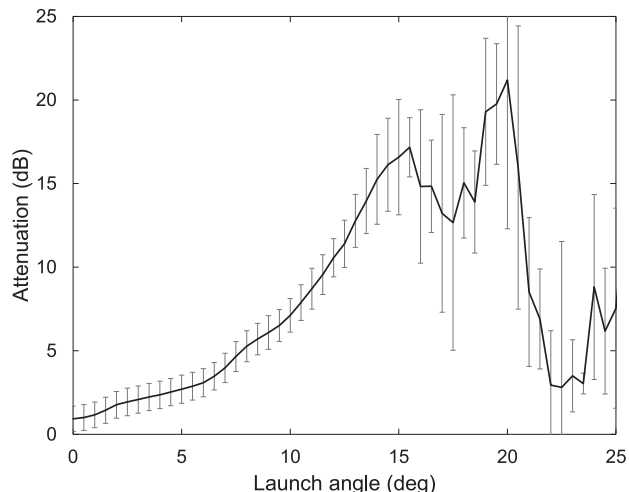
By replacing the cylindrical lens with a plano-convex lens (60 mm focal length, limited by the spacing of the rotation/translation stages), focused rays (i.e., equivalent to a mixture of different meridional ray groups) centered on the sensing fiber with a divergence of 1.7 deg was generated at the input of the sensing fiber. The attenuation was measured to be 3.7 dB. By sweeping θ, the attenuation can be as high as 23.1 dB. However, there are slight center offsets due to the imperfect centering of the fiber end on the rotation stage, leading to skew-ray generation and unrepresentative results.

To summarize and compare the different types of fiber excitation (i.e., same laser power was used), LSSR possess the best performance for an evanescent-wave-based bio/chemical sensor, while normal-incidence rays exhibit the worst performance. Table I lists the maximum attenuation associated with each excitation type, as well as the experimental conditions, and the repeatability of the measurements. The repeatability is anticipated to improve with fiber coatings instead of dye baths, because fluid dynamics can affect pump absorption due to optical forces and evaporation-induced concentration changes. Relative to collimated meridional rays, LSSR yields an enhancement of ~4.7 dB or factor of ~3. Compared with collimated skew rays, LSSR provides an enhancement of ~14 dB or factor of ~20 (i.e., one order of magnitude). This level of improvement is more than the approximate theoretical upper limit of 160 um (fiber radius) / 40 um (light-sheet thickness) = ~4, possibly due to several reasons: (a) stronger optical forces associated with the higher intensity of LSSR pulled fluorophores closer to the surface of the sensing fiber that absorbed more pump light; and (b) nonlinear effects associated with the higher intensity of LSSR led to self-focusing, and thus reduced the light-ring thickness. This intriguing possibility will be investigated in future work.

Relative to focused rays, LSSR benefits from an enhancement of ~26 dB. Compared to normal-incidence rays, LSSR facilitates an enhancement of ~34 dB or factor of ~2500 (i.e., three orders of magnitude). This enhancement with LSSR would be

TABLE I
COMPARISON OF DIFFERENT EXCITATION TYPES

| Excitation type	Measured attenuation (dB)	Repeatability (%)
Light-sheet skew rays (collimated)	34.9 (20.0 deg, 12.5 μm) 32.0 (17.0 deg, 112.5 μm)	~5
Meridional rays (collimated)	30.2 (21.5 deg, 0 μm)	~5
Skew rays (collimated)	21.2 (20.0 deg) 17.2 (15.5 deg)	~13
Focused rays (tilted, centered) [9]	~19 higher than normal-incidence (1.7 deg)	N/A
Focused rays (centered)	8.5 (1.7 deg)	~3
Normal-incidence rays	0.9 (0 deg)	~13

Fig. 7. Measured attenuation of light-sheet skew rays as a function of polarization azimuth relative to the plane of fiber rotation. Inset: relationship between dye concentration and attenuation.

even larger if the sensing fiber was kept straight. As expected, this level of improvement (~34 dB) is higher than that of focused, tilted and centered rays (~19 dB) [9]. The two orders of magnitude enhancement offered by collimated skew rays over normal-incidence rays shows excellent agreement with previous work on refractometers [30]. Surprisingly, it was observed that collimated meridional rays outperform collimated skew rays that is a mixture of different ray groups. This is likely due to the far greater penetration depth experienced by light.

The final stage of optimization (i.e., building on 20.0 deg, 12.5 μm) for LSSR is polarization azimuth. It was not previously explored for each of the excitation types, because the improvement in attenuation is similar for all types. Figure 7 reveals the consistent attenuation from P-polarized to S-polarized light (i.e., prior measurements), which varies by no more than 0.3 dB. This quality can be used to increase the tolerance of sensors to the polarization azimuth. The repeatability is ~5%, which corresponds to attenuation error bars of ± 0.4 dB. The polarization error bars are ± 2 deg.

As a potential evanescent-wave-based bio/chemical sensor, the highest sensitivity with LSSR, 40 mm functionalized fiber length and 320 μm core diameter was measured to be 34.9 dB/(mg/ml) or 8.73 dB/(mg/ml)/cm, based on the slope of attenuation measured at Rhodamine B concentrations of 0.1 μg/ml, 1 μg/ml, 10 μg/ml, 100 μg/ml and 1 mg/ml. The repeatability is ~5%, which corresponds to attenuation error bars of ± 0.4 dB. The corresponding detection limit is calculated to be 24.9 ng/ml, from dividing the noise-equivalent attenuation (8.7×10^{-4} dB based on 10 nW noise amplitude and 50 μW baseline power over 3 min) by the sensitivity. Note the results correspond to specific fiber dimensions/geometry/ materials/bend angles, and re-optimization is needed if there are changes.
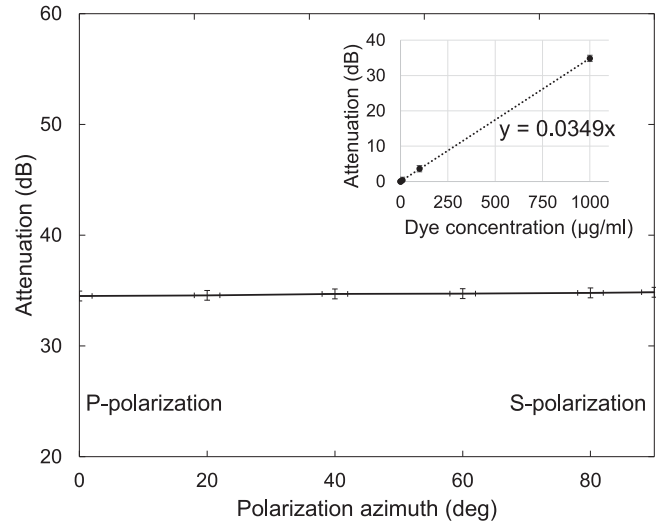
To increase the sensitivity and thus improve the detection limit, the following should be considered: (a) A longer section of functionalized sensing-fiber; (b) Better optics (e.g., less spherical aberration) for narrowing the light-sheet thickness and divergence angle; (c) Larger fiber diameter; and (d) Minimize the fiber refractive-index and thus numerical aperture (i.e., supports γ just up to optimum launch conditions) of the sensing fiber to scale up the penetration depth and thus attenuation for all launch conditions. However, for fluorescence collection, a higher numerical-aperture is desirable.

VI. CONCLUSIONS

To improve evanescent-wave-based bio/chemical sensors, we have demonstrated a new sensing technique with light-sheet excitation of skew rays in a multimode fiber (40 mm functionalized fiber length, 320 μm core diameter), and compared it with other excitation methods in terms of attenuation of pump light through Rhodamine B. We showed that the attenuation obtained through light-sheet excitation (i.e., normalized sensitivity of 8.73 dB/(mg/ml)/cm) of the optimum skew ray group can be up to three orders of magnitude higher than those of other excitation types, such as collimated meridional rays, collimated skew rays, focused-centered rays, focused-tilted-centered and normal-incidence rays. It can be extended to enhance the sensitivity of a variety of sensing mechanisms including optical-confinement absorption, molecular (e.g., pump) absorption, or fluorescence. This is an inline configuration based on commercial optics and multimode fibers that can be highly sensitive, relatively temperature insensitive, and highly robust.

REFERENCES

[1] E. P. Schartner, G. Tsiminis, M. R. Henderson, S. C. Warren-Smith, and T. M. Monro, "Quantification of the fluorescence sensing performance of microstructured optical fibers compared to multi-mode fiber tips," *Opt. Express*, vol. 24, no. 16, pp. 18541–18550, Aug. 2016.

[2] M. Yokata and T. Yoshino, "Optical fiber water droplet sensor using absorption of fluorescence of Tm^{3+}:YAG," *Appl. Opt.*, vol. 37, no. 13, pp. 2526–2533, May 1998.

[3] "Fluorescence sensing," in *Principles of Fluorescence Spectroscopy*, 1st ed., J. R. Lakowicz, Ed. Boston, MA, USA: Springer, pp. 623–673, 2006.

[4] L. Liu *et al.*, "TriPleXTM waveguide-based fuorescence biosensor for multichannel envrionmental contaminants detection," *Biosensors Bioelectronics*, vol. 106, pp. 117–121, Feb. 2018.

[5] R. A. Lieberman, L. L. Blyler, and L. G. Cohen, "A distributed fiber optic sensor based on cladding fluorescence," *J. Lightw. Technol.*, vol. 8, no. 2, pp. 212–220, Feb. 1990.

[6] O. S. Wolfbeis, "Fluorescence optical sensors in analytical chemistry," *Trends Anal. Chem.*, vol. 4, no. 7, pp. 184–188, Aug. 1985.

[7] K. Muto, "Electric-discharge sensor utilizing fluorescent optical fiber," *J. Lightw. Technol.*, vol. 7, no. 7, pp. 1029–1032, Jul. 1989.

[8] G. D. Peng, Z. Xiong, and P. L. Chu, "Fluorescence decay and recovery in organic dye-doped polymer optical fibers," *J. Lightw. Technol.*, vol. 16, no. 12, pp. 2365–2372, Dec. 1998.

[9] A. Messica, A. Greenstein, and A. Katzir, "Theory of fiber-optic, evanescent-wave spectroscopy and sensors," *Appl. Opt.*, vol. 35, no. 13, pp. 2274–2284, May 1996.

[10] R. Wang, Y. Xiang, X. Zhou, L. Liu, and H. Shi, "A resusable aptamer-based evanescent wave all-fiber biosensor for highly sensitive detection of ochratoxin A," *Biosensors Bioelectronics*, vol. 66, pp. 11–18, Feb. 2015.

[11] R. Venkataraj, V. P. N. Nampoorimpoori, P. Radhakrishnan, and M. Kailasnath, "Chemically tapered multimode optical fiber probe for fluoride detection based on fluorescence quenching of curcumin," *IEEE Sens. J.*, vol. 15, no. 10, pp. 5584–5591, Jun. 2015.

[12] J. Ma and W. J. Bock, "Dramatic performance enhancement of evanescent-wave multimode fiber fluorometer using non-Lambertian light diffuser," *Opt. Express*, vol, 15, no. 25, pp. 16457–16470, Dec. 2007.

[13] G. Y. Chen, C. A. Codemard, P. M. Gorman, J. S. Chan, and M. N. Zervas, "Angle-resolved characterization and ray-optics modeling of fiber-optic sensors," *J. Lightw. Technol.*, vol. 33, no. 24, pp. 5210–5217, Dec. 2015.

[14] G. Herskowitz, H. Kobrinski, and U. Levy, "Optical power distribution in multimode fibers with angular-dependent mode coupling," *J. Lightw. Technol.*, vol. 1, no. 4, pp. 548–554, Dec. 1983.

[15] D. Su, A. A. P. Boechat, and J. D. C. Jones, "Beam delivery by large-core fibers: Effect of launching conditions on near-field output profile," *Appl. Opt.*, vol. 31, no. 27, pp. 5816–5821, Sep. 1992.

[16] D. Feuermann, J. M. Gordon, and M. Huleihil, "Light leakage in optical fibers: Experimental results, modeling and the consequences for solar concentrators," *Sol. Energy*, vol. 72, no. 3, pp. 195–204, Oct. 2002.

[17] C. Pask, "Generalized parameters for tunneling ray attenuation in optical fibers," *J. Opt. Soc. Amer. B.*, vol. 68, no. 1, pp. 110–116, Jan. 1978.

[18] L. Allen and M. Padgett, "The phenomenology of orbital angular momentum," in *Twisted Photons: Applications of Light With Orbital Angular Momentum*, 1st ed. J. P. Torres and L. Torner, Eds. Hoboken, NJ, USA: Wiley, 1983, Ch. 1.2.

[19] G. Y. Chen, S. Shahnia, T. M. Monro, and D. G. Lancaster, "Force sensors using skew-ray-probed plastic optical fibers," *IEEE Photon. J.*, vol. 10, no. 3, Jun. 2018, Art. no. 6802208.

[20] M. Archenault, H. Gagnaire, J. P. Goure, and N. Jaffrezic-Renault, "A simple intrinsic optical fibre refractometer," *Sens. Actuators B, Chem.*, vol. 5, no. 1, pp. 173–179, Aug. 1991.

[21] J. Ma, W. J. Bock, and A. Cusano, "Insights into tunnelling rays: Outperforming guided rays in fiber-optic sensing device," *Opt. Express*, vol. 17, no. 9, pp. 7630–7639, Apr. 2009.

[22] Y. Xu, N. B. Jones, J. C. Fothergill, and C. D. Hanning, "Theoretical analysis of the evanescent wave absorption coefficient for multimode fibre-optic evanescent wave absorption sensors," *J. Modern Opt.*, vol. 46, no. 14, pp. 2007–2017, Jul. 2009.

[23] G. Y. Chen, D. Otten, Y. Q. Kang, T. M. Monro, and D. G. Lancaster, "Measuring the radial position of internal defects within optical fibers using skew rays," *J. Sens.*, vol. 2017, Jun. 2017, Art. no. 4879528.

[24] R. L. Dean, "Understanding Beer's law: An interactive laboratory presentation and related exercises," *J. Lab. Chem. Educ.*, vol. 2, no. 3, pp. 44–49, Jan. 2014.

[25] V. Benolt and M. C. Yappert, "Effect of capillary properties on the sensitivity enhancement in capillary/fiber optical sensors," *Anal. Chem.*, vol. 68, no. 1, pp. 183–188, Jan. 1996.

[26] J. Tripathi, A. Sharma, S. Tripathi, and K. K. Das, "Concentration dependent optical properties of rhodamine B doped poly(vinyl alcohol) solutions," *Macromolecular Res.*, vol. 24, no. 7, pp. 617–622, Jul. 2016.

[27] M. Gong, Y. Yuan, C. Li, P. Yan, H. Zhang, and S. Liao, "Numerical modeling of transverse mode competition in strongly pumped multimode fiber lasers and amplifiers," *Opt. Express*, vol. 15, no. 6, pp. 3236–3246, Mar. 2007.

[28] "Focusing and collimating," Tech. Notes, 2018. [Online]. Available: https://www.newport.com/n/focusing-and-collimating

[29] A. Müller, M. C. Wapler, and U. Wallrabe, "Segmented Bessel beams," *Opt. Express*, vol. 25, no. 19, pp. 22640–22647, Sep. 2017.

[30] G. Y. Chen *et al.*, "Enhanced responsivity with skew ray excitation of reflection- and transmission-type refractometric sensors," *Opt. Lett.*, vol. 39, no. 13, pp. 3822–3825, Jul. 2014.

Authors' biographies not available at the time of publication.